Investigation of the Scale Similarity Principle for Subgrid Modelling of the Reactive Richtmyer-Meshkov Instability

M. Bambauer, J. Hasslberger and M. Klein
Institute of Applied Mathematics and Scientific Computing, Bundeswehr University Munich, Neubiberg, Germany

1 Introduction

The accurate prediction of explosion loads in industry scale accident scenarios, as often found in nuclear and process plant safety, poses a major challenge due to the large spectrum of time and length scales involved. The Richtmyer-Meshkov instability (RMI) can be a significant factor, contributing to flame acceleration and possibly detonation in geometrically confined explosions due to the interaction of shock waves and flames [1]. The RMI is characterized by a heavy build up of baroclinic torque across the disturbed flame brush, causing a severe increase in flame wrinkling, greatly increasing the flame surface and the integral reaction rate. The precise calculation of chemical reaction rates, small scale wrinkles and the shock propagation itself impose high requirements on the resolution (both in time and space) and discretization schemes. While direct numerical simulations (DNS) allow the effects of the reactive RMI to be simulated accurately, the computational demands of a large scale simulation in an industrial context make such simulations unfeasible, hence necessitating lower resolved unsteady Reynolds-Averaged Navier-Stokes (URANS) or Large Eddy Simulations (LES). Accordingly, the small scale effects of the RMI have to be introduced into the URANS or LES via a suitable subgrid model. In this work data from hydrogen/air shock-flame DNS is utilized to develop modelling approaches based on fractal theory and the scale similarity principle, which allow the reconstruction of the subgrid flame wrinkling from the data present in low-fidelity simulations.

2 Computational method

The direct numerical simulations of the hydrogen/air shock-flame interactions are performed using the compressible 3D combustion code SENGA [2]. The chemical source term is expressed by a one-step irreversible Arrhenius-type approach, which allows to capture the effects of the reactivity on the mainly fluid dynamics dominated RMI, while avoiding the large computational costs encountered with detailed chemistry approaches. The 5th order WENO-5 spatial discretization scheme [3] is utilized due to its minimal-dissipation and oscillation free shock capturing capabilities. For temporal discretization a 3rd order Runge-Kutta scheme is used. Fig. 1 shows the simulation domain, which consists of a rectangular channel containing

Correspondence to: maximilian.bambauer@unibw.de

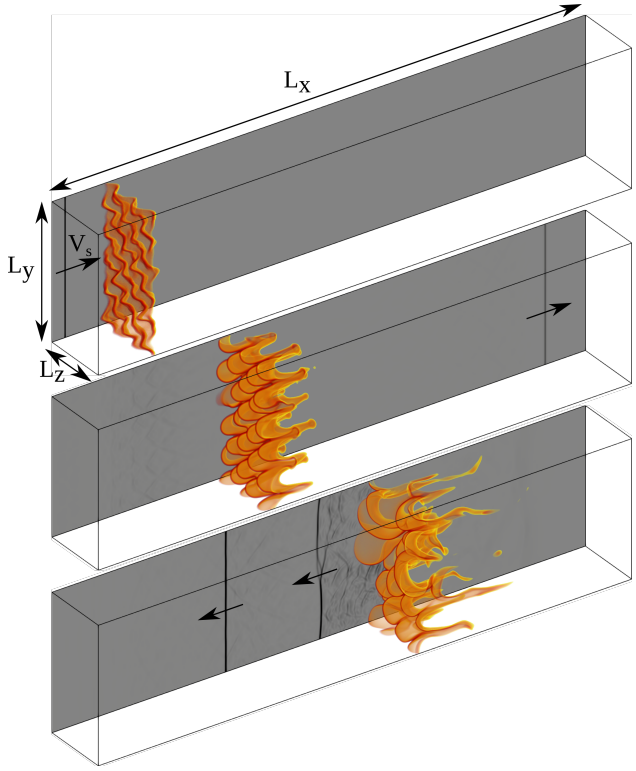

Figure 1: Simulation setup for equivalence ratio $\phi = 1.0$, with shock propagating from left to right and statistically planar flame at $t = 0$ (top). Flame wrinkling after first shock interaction (middle) and after first and second reshock interaction (bottom). Flame is shown as semitransparent iso-volume (varying opacity) of reaction progress variable c (constrained by $c = 0.15$/dark red and $c = 0.85$/bright yellow). Background slice shows pressure gradient magnitude (grayscale).

a statistically planar flame and a planar shock wave. After interacting with the flame the shock is reflected by an adiabatic wall boundary, causing a reshock interaction. Subsequent interactions occur due to additional reflections of the shock from the wall and the flame surface itself. The flame is initially disturbed using a single mode base oscillation superimposed with multimode oscillations of smaller amplitudes [4]. This allows for a well defined base disturbance, while the symmetry is being broken up by a quasi-stochastic disturbance of the flame front.

The set-up properties for the hydrogen/air mixture are calculated at $T_0 = 298.15K$ and $p_0 = 1$bar using the GRI-MECH 3.0 database implemented in the Cantera toolkit. In earlier work [5] the effects of variations in shock Mach number M_s and flame disturbance wavelength on the RMI development were analysed for a nonreactive case. For the present work $M_s = 1.5$ and the initial flame disturbance is kept constant, while the equivalence ratio of the reactive hydrogen/air flame is varied between $\phi = 1.0$ (stoichiometric) and $\phi = 0.5$ (very lean). For the gas-mixture an effective Lewis number $\mathrm{Le}_{\mathrm{eff}}$ [6] is defined (valid for $\phi \leq 1$) as

$$\mathrm{Le}_{\mathrm{eff}} = 1 + \frac{(\mathrm{Le}_{\mathrm{O}_2}(\phi) - 1) + (\mathrm{Le}_{\mathrm{H}_2}(\phi) - 1)A_{\mathrm{Le}}}{1 + A_{\mathrm{Le}}}\,, \tag{1}$$

where $A_{\mathrm{Le}} = 1 + \beta_z(\max(1/\phi, \phi) - 1)$, with the Zeldovich number $\beta_z = 5$. The values for the hydrogen

Lewis number $\mathrm{Le}_{\mathrm{H}_2}(\phi)$ and the oxygen Lewis number $\mathrm{Le}_{\mathrm{O}_2}(\phi)$ are aquired with Cantera at the respective equivalence ratio ϕ. Ensuring a sufficient resolution of the thermal flame thickness, initial flame distortion and flame wrinkling the domain is discretized by $1024 \times 256 \times 128$ grid points, which normalized by the thermal flame thickness $\delta_{\mathrm{th,st}}$ of the stoichiometric case results in dimensions of $L_\mathrm{x} \times L_\mathrm{y} \times L_\mathrm{z} = 128\delta_{\mathrm{th,st}} \times 32\delta_{\mathrm{th,st}} \times 16\delta_{\mathrm{th,st}}$. The LES are based on the DNS setup, where the grid size (Δ_{LES}) has been increased to $2\Delta_{\mathrm{DNS}}$, $4\Delta_{\mathrm{DNS}}$ and $8\Delta_{\mathrm{DNS}}$.

With the Arrhenius model the chemical source term $\dot{\omega}$ of the reaction progress variable transport equation can be expressed as

$$\dot{\omega} = \rho B(1-c)\mathrm{exp}\left[\frac{-E_\mathrm{ac}}{RT}\right] , \tag{2}$$

where B, E_ac and R denote the pre-exponential factor, the activation energy and the molar gas constant. At lower resolutions Eq. (2) becomes increasingly less accurate, as the thermal flame thickness cannot be resolved sufficiently anymore. To circumvent this issue, one attractive possibility is to utilize a flame surface density (FSD) approach and express the filtered chemical source term denoted with $\bar{\dot{\omega}}_{\mathrm{FSD}}$ as

$$\begin{aligned} \bar{\dot{\omega}}_{\mathrm{FSD}} &= \bar{\rho}_{\mathrm{ub,0}} S_{\mathrm{L,0}} F(\bar{c}) |\nabla \bar{c}| \Xi \, , \\ \Xi &= \Xi_\rho \Xi_{S_\mathrm{L}} \Xi_\mathrm{w} \, , \end{aligned} \tag{3}$$

where $\bar{\rho}_{\mathrm{ub,0}}$ and $S_{\mathrm{L,0}}$ denote the unburned density and unstretched laminar flame speed at the reference conditions. The total correction term Ξ includes the density correction Ξ_ρ, the laminar flame speed correction Ξ_{S_L} and the subgrid wrinkling Ξ_w. The generalised flame surface density is defined by $\overline{|\nabla c|} = |\nabla \bar{c}| \Xi_\mathrm{w}$, with $\bar{c}$ as the LES-filtered reaction progress variable. The function $F(\bar{c}) = C_\mathrm{R}\bar{c}(1-\bar{c})$ reduces flame thickening due to diffusion, as usually encountered with the FSD-approach. The factor $C_\mathrm{R} = 6$ is chosen so that $\int_V F(\bar{c}) dV \approx 1$, therefore acting as a neutral element in the calculation of the integral reaction rate. While changes of the unburned values for pressure, density and temperature (due to the shock interaction) are implicitly included in the Arrhenius approach, they have to be considered explicitly in the FSD-approach, by adding the correction terms Ξ_ρ and Ξ_{S_L}. The term $\Xi_\rho = (p/p_0)^{1/\gamma}$ uses the isentropic relation to approximate the corrected unburned density $\rho_{\mathrm{ub}} = \rho_{\mathrm{ub,0}}\Xi_\rho$ from the partially burned states of the flame, without the need for an explicit shock treatment. The effects of the shock are implicitly included in the pressure values p. The laminar flame speed correction $\Xi_{S_\mathrm{L}} = (T_{\mathrm{ub}}/T_{\mathrm{ub,0}})^{\alpha_\mathrm{T}}(p_{\mathrm{ub}}/p_{\mathrm{ub,0}})^{\beta_\mathrm{p}}$ adds the dependency of the laminar flame speed to temperature and pressure changes, where the unburned temperature is again calculated using the isentropic relation $T_{\mathrm{ub}} = T_{\mathrm{ub,0}}(p_{\mathrm{ub}}/p_0)^{(\gamma-1)/\gamma}$ and it is assumed that $p_{\mathrm{ub}} = p$. The exponents α_T and β_p are functions of T_{ub} and p_{ub} using the correlations of Hu *et al.* [7].

The validity of the correction terms Ξ_ρ and Ξ_{S_L} can be verified with the DNS data via an a-priori analysis of Damköhler's hypothesis, which postulates $S_\mathrm{T}/S_\mathrm{L} = A_\mathrm{T}/A_\perp$ for unity Lewis numbers. With A_T as the turbulent flame area and $A_\perp$ as the projected flame area, the turbulent and laminar flame speeds can be expressed as $S_\mathrm{T} = \int_V (\dot{\omega}/(\rho_{\mathrm{ub,0}}\Xi_\rho) dV/A_\perp$ and $S_\mathrm{L} = S_{\mathrm{L,0}}\Xi_{S_\mathrm{L}}$, respectively. As shown in Fig. 2 (left), applying the correction terms leads to a major reduction in the departure from Damköhler's hypothesis, which indicates that the terms successfully account for shock effects in the reactive source term of the FSD-model. As the hypothesis is only strictly valid for $\mathrm{Le}_{\mathrm{eff}} = 1$, a deviation for lean mixtures ($\mathrm{Le}_{\mathrm{eff}} \ll 1$) is to be expected (Fig. 2,right). In these cases the agreement can be improved by adding an additional Lewis number correction in the form of $S_\mathrm{L} = S_{\mathrm{L,0}}\Xi_{S_\mathrm{L}}\Xi_{\mathrm{Le}}$, with $\Xi_{\mathrm{Le}} = 1/\mathrm{Le}_{\mathrm{eff}}$. For brevity Sec. 3 will focus on the stoichiometric case ($\phi = 1.0$), but additional results for the lean case ($\phi = 0.5$) will be shown at the conference.

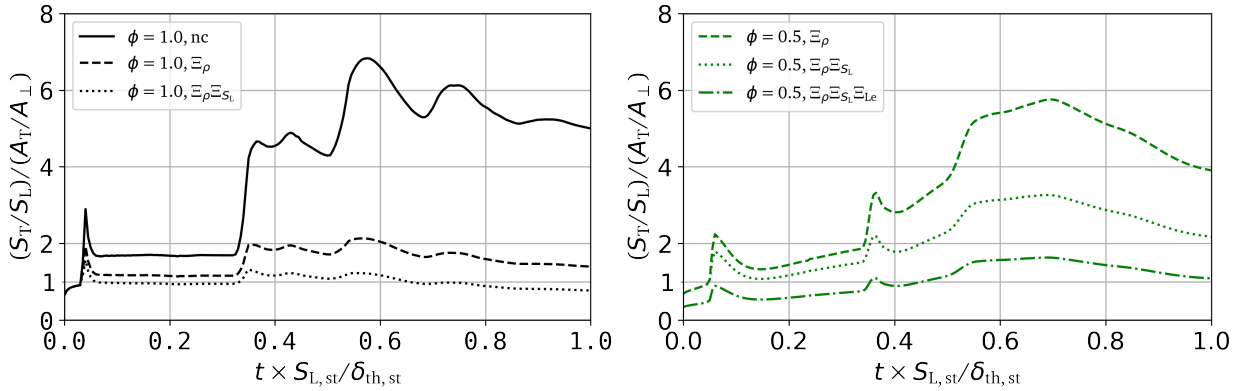

Figure 2: Deviation from the idealized Damköhler hypothesis for $\phi = 1.0$ (left) and $\phi = 0.5$ (right). Influence of the correction terms (nc: no correction term) for the unburned density (Ξ_ρ), laminar flame speed (Ξ_{S_L}) and the Lewis number correction (Ξ_{Le}).

3 Results and discussion

Figure 3 compares the effect of the Ξ terms on the development of the normalized integral reaction rate $\int_V \dot{\omega} dV/(S_{L,0}\rho_{ub,0}A_\perp)$ for an a-posteriori analysis (implicit LES without other subgrid-scale models) using different grid sizes. Without any correction terms applied ($\Xi = 1$) there is a large gap between the DNS and LES cases. Briefly summarized there are two reasons for this: (i) As the analysis of Damköhler's hypothesis has shown, the reaction rate is severely underestimated by the FSD model, when the Ξ_ρ and Ξ_{S_L} correction terms are not applied (Fig. 2) and (ii) Without the wrinkling factor Ξ_w the small scale flame wrinkling and therefore the flame area itself is underestimated, as it cannot be properly resolved at such resolutions. For the present type of perturbation another effect can be observed for grid sizes beyond $4\Delta_{DNS}$, as the initial flame perturbation cannot be captured by the grid anymore and the flame becomes essentially planar. To further emphasize that effect, an additional case without initial disturbance ('nd' case) is investigated. At $8\Delta_{DNS}$ the development with and without initial disturbance is identical up to $t \times S_{L,st}/\delta_{th,st} \approx 0.5$, where the curves start to diverge. This is most likely due to very small disturbances being enhanced by the RMI, causing the quasi planar flame to become unstable and fold up at later stages of the simulation. As the $8\Delta_{DNS}$ case is an outlier it is omitted from the following discussion.

The inclusion of the Ξ_ρ and Ξ_{S_L} correction terms already leads to a great improvement for both cases, with some deviations from the DNS results after the first shock interaction (for $4\Delta_{DNS}$) and bigger deviations following the reshock interaction. It can be inferred from the a-priori analysis shown in Fig. 2 that the best match of filtered and unfiltered reaction rates is achieved for $t \times S_{L,st}/\delta_{th,st} < 0.3$. While the agreement is still acceptable after the reshock, there are deviations up to $\pm 20\%$ from Damköhler's hypothesis. Applied to the a-posteriori analysis of the integral reaction rate in Fig. 3 this means that (leaving aside the influence of subgrid wrinkling Ξ_w) a slight underestimation (y-axis > 1 in Fig. 2), or overestimation (y-axis < 1 in Fig. 2) of the integral reaction rate is to be expected after the reshock.

The wrinkling factor $\Xi_w = A_T/A_\perp$ is modeled using a fractal power law approach $\Xi_w = (\eta_o/\eta_i)^{D_f-2}$, where η_o and η_i are the outer and inner cut-off scales and D_f is the fractal dimension. Assuming for the present cases that $\eta_i \approx \Delta_{DNS}$, the ratio η_o/η_i can be evaluated to $\eta_o/\eta_i = 2$ and $\eta_o/\eta_i = 4$, respectively. Generally Ξ_w and D_f can be obtained from $\Xi_w = \overline{|\nabla c|}/|\nabla \bar{c}|$ by explicitly filtering the DNS data [8]. In the LES-cases this approach is not possible as only the filtered data is accessible. A scale-similarity approach is

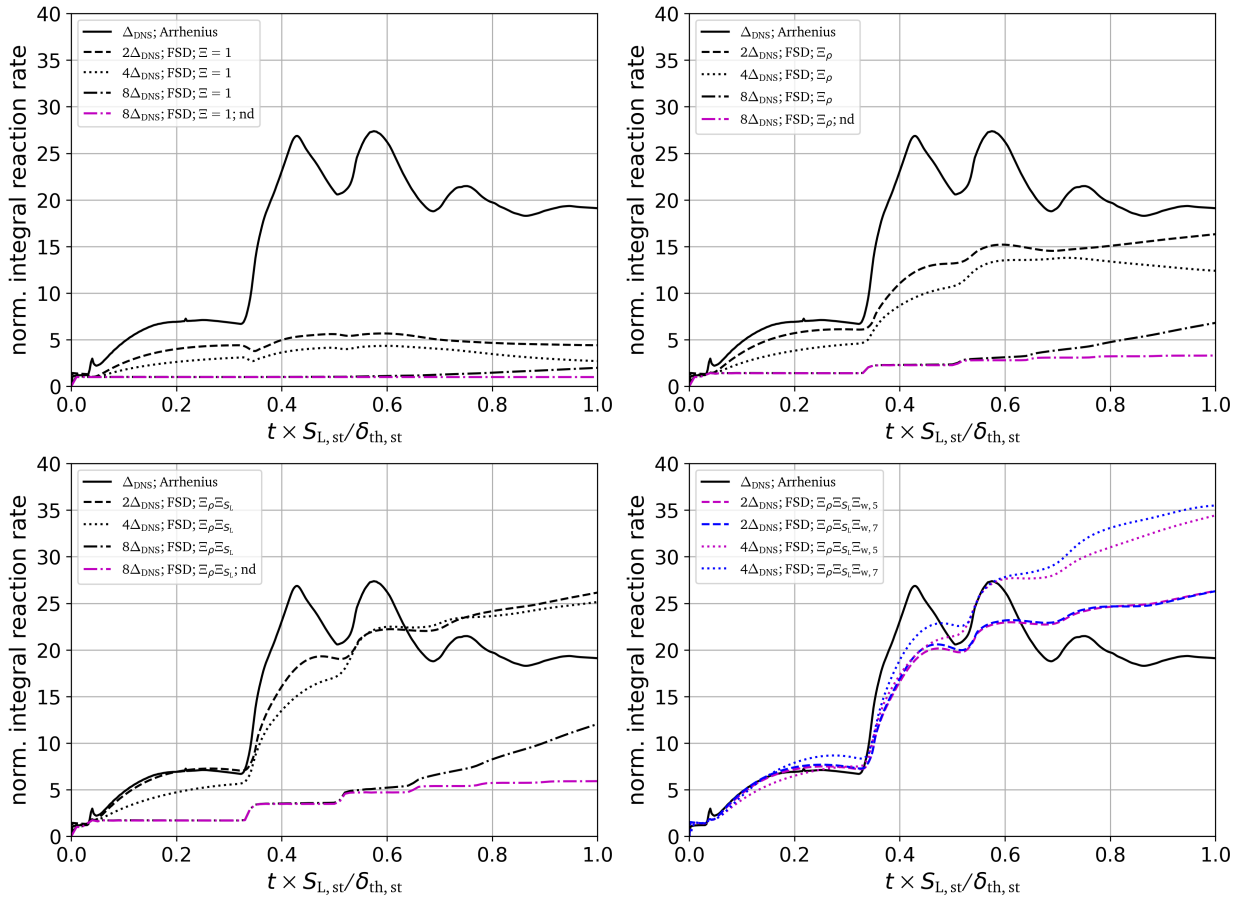

Figure 3: Normalized integral reaction rate over time for $\phi = 1.0$ and different grid sizes Δx (nd: case without flame distortion). Top: No correction terms Ξ applied (left) and with corrected unburned density (right). Bottom: Correction to unburned density and laminar flame speed (left) and all corrective terms applied including the flame wrinkling factor Ξ_w (right) for normalized test filter sizes 5 and 7.

utilized to extract the subgrid wrinkling factor Ξ_w from the resolved wrinkling $\Xi_{ss} = \widehat{|\nabla \bar{c}|}/|\nabla \hat{\bar{c}}|$ (assuming $D_f = D_{f,ss}$), where $\hat{c}$ denotes the application of a test filter (boxfilter). The wrinkling factor Ξ_w is then obtained from

$$\Xi_w = (\eta_o/\eta_i)^{\frac{\ln(\Xi_{ss})}{\ln(\Delta_f/\Delta_{LES})}} , \tag{4}$$

with Δ_f/Δ_{LES} denoting the ratio of the test filter size Δ_f to the LES filter width Δ_{LES}. Figure 3 (bottom right) shows the effect of the Ξ_w term for an explicit boxfilter with $\Delta_f = 5\Delta_{LES}$ and $\Delta_f = 7\Delta_{LES}$, for $\Delta_{LES} = 2\Delta_{DNS}$ and $\Delta_{LES} = 4\Delta_{DNS}$, respectively. After the first shock interaction all cases show a good match with the DNS data and the prediction is significantly improved for the reshock as well. As the resolution is decreased the influence of the Ξ_w term increases. While the deviations towards the end can be partly explained by the previously mentioned deviations from Damköhler's hypothesis, another aspect can be the diffusive flame thickening encountered in FSD models. While this effect is diminished by the $F(c)$ term in Eq. (3) the correction term may become inaccurate for highly wrinkled surfaces and repeated shock-flame interactions.

4 Conclusions and outlook

DNS of hydrogen/air shock-flame interactions are performed to calculate the increase of flame wrinkling and integral reaction rate as caused by the reactive RMI. In lower resolved LES it is found that the modelling of the reactive source term (FSD model) can be greatly improved by applying corrections for the unburned gas quantities Ξ_ρ, the laminar flame speed Ξ_{S_L} and the subgrid flame wrinkling Ξ_w. The flame wrinkling Ξ_w can be extracted from the LES-data by applying a test filter, assuming scale similarity in the resolved flame wrinkling and the subgrid scales. The Ξ terms greatly improve the model prediction of the integral reaction rate, especially after the first and second shock-flame interaction. At later times an offset between LES and DNS data becomes apparent, which can be attributed to inaccuracies in the Ξ correction terms and artificial diffusion encountered with the FSD model. For brevity only stoichiometric flames were considered in this work. Additional work (presented at the conference) will also focus on lean gas mixtures, which are important as they are commonly encountered in industrial explosion scenarios.

The presented work is funded by the German Federal Ministry of Economic Affairs and Energy (BMWi) on the basis of a decision by the German Bundestag (project no. 1501574) which is gratefully acknowledged.

References

[1] Khokhlov, A. M., Oran, E. S., Thomas, G. O. (1999). Numerical simulation of deflagration-to-detonation transition: The role of shock-flame interactions in turbulent flames. Combustion and Flame, 117(1–2), 323-339.

[2] Jenkins, K. W., Cant, R. S. (1999). Direct Numerical Simulation of Turbulent Flame Kernels. Recent Advances in DNS and LES, Fluid Mechanics and its Applications, 54, 191–202. Springer, Dordrecht (ISBN 978-94-011-4513-8).

[3] Jiang, G.-S., Shu, C.-W. (1996). Efficient Implementation of Weighted ENO Schemes. Journal of Computational Physics, 126(1), 202-228.

[4] Tritschler, V. K., Hickel, S., Hu, X. Y., Adams, N. A. (2013). On the Kolmogorov Inertial Subrange Developing from Richtmyer-Meshkov Instability. Physics of Fluids, 25, 071701.

[5] Bambauer, M., Hasslberger, J., Klein, M. (2020). Direct Numerical Simulation of the Richtmyer-Meshkov Instability in Reactive and Nonreactive Flows. Combustion Science and Technology, 192(11), 2010-2027.

[6] Bechtold, J. K., Matalon, M. (2001). The Dependence of the Markstein Length on Stoichiometry. Combustion and Flame, 127, 1906-1913.

[7] Hu, E., Huang, Z., He, J., Miao, H. (2009). Experimental and numerical study on laminar burning velocities and flame instabilities of hydrogen–air mixtures at elevated pressures and temperatures. International Journal of Hydrogen Energy, 34(20), 8741-8755.

[8] Bambauer, M., Chakraborty, N., Klein, M., Hasslberger, J. (2021). Vortex dynamics and fractal structures in reactive and nonreactive Richtmyer–Meshkov instability. Physics of Fluids, 33(4), 044114.